ISSN 1070-3284, Russian Journal of Coordination Chemistry, 2018, Vol. 44, No. 7, pp. 415–420. © Pleiades Publishing, Ltd., 2018.

Magnetism and Photocatalytic Degradation of Organic Dyes Based on a New Metal Formate Framework[1]

F. M. Wang[a], B. H. Li[b], Z. D. Luo[b], J. Q. Liu[b], H. Sakiyama[c], and A. Q. Ma[b, *]

[a] *Department of Chemistry and Chemical Engineering, Shaanxi Xueqian Normal University, Xian, P.R. China*

[b] *Key Laboratory for Research and Development of New Medical Materials of Guangdong Medical University, Dongguan Key Laboratory of Drug Design and Formulation Technology, School of Pharmacy, Guangdong Medical University, Dongguan, 523808 P.R. China*

[c] *Department of Material and Biological Chemistry, Faculty of Science, Yamagata University, Kojirakawa, Yamagata 990-8560 Japan*

**e-mail: maqandght@126.com*

Received August 28, 2017

Abstract—A new MOF of $[Co(HCOO)_2] \cdot 0.33DMF$ (**I**) was prepared and characterized by IR, powder X-ray diffraction, and single-crystal X-ray diffraction (CIF file CCDC no. 1571166). Complex **I** exhibits a diamond framework based on Co-centered $CoCo_4$ tetrahedral nodes, in which all metal ions have octahedral coordination geometry and all HCOO groups link the metal ions in *syn-syn/anti* modes. The magnetic property shows a main antiferromagnetic interaction and the ferromagnetic phase transition below 2 K. Furthermore, the photocatalytic properties of **I** for degradation of the methyl violet and Rhodamine B have been explored.

Keywords: magnetism, formate, photocatalytic property

DOI: 10.1134/S1070328418070011

INTRODUCTION

Metal-organic frameworks (MOFs) have received a wide range of attention in the field of supramolecular chemistry and crystal engineering, owing to their intriguing aesthetic structures and their potential applications (such as, host–guest chemistry and magnetic materials) [1–5]. Ligands with carboxylate groups are employed most often in the design and synthesis of MOFs. For example, benzene polycarboxylate acids can bind to and connect metal centers in various modes to generate complexes with different magnetic properties. However, formate anions, $HCOO^-$, which is the simplest carboxylate, has been used infrequently as a building block [6–22]. More porous formate coordination polymers, a series of $[M^{II}_3(HCOO)_6]$ formate-MOFs were synthesized and their magnetic properties were studied [23–29]. A good example is the MOFs with a general formula cation@$M(HCOO)_3$ (cation = alkylammonium, M = divalent metal ion). These MOFs undergo a ferroelectric (or antiferroelectric) phase transition in the temperature range of 160–185 K, depending on the involved M(II). They also exhibit a canted antiferromagnetic ordering at low temperatures (T_c = 8–36 K) [30–34].

On the other hand, dimethyl formamide (DMF) usually takes as a polar solvent. It is reported that the C–N bond cleavage becomes easy under acidic conditions [27–31], and its decomposition product, formic acid (HCOOH), is a good bridging ligand for constructing MOFs; consequently, the relative coordination compounds involving the formate ligand have been numerously reported. Recently, we have devoted to the systematic investigation on assembly of Mn-MOFs induced by temperature-driven C–N bond cleavage of DMF molecules [35–40]. This success prompted us to look for analogues with other divalent transition metals. Our motives are as follows: (a) to control the pore size by using divalent cations having different radii (for example, Mn (0.95 Å), Co (0.80 Å)), and (b) to study the magnetic interactions by changing the electronic configuration [41]. We reported here the successful synthesis of the cobalt MOF of $[Co(HCOO)_2] \cdot 0.33DMF$ (**I**) [42]. The magnetic property shows a main antiferromagnetic interaction and the ferromagnetic phase transition below 2 K. Furthermore, the photocatalytic properties of **I** for degradation of the methyl violet (MV) and Rhodamine B (RhB) have been explored.

[1] The article is published in the original.

Table 1. Crystallographic data and structure refinement for complex **I**

Parameter	Value
Formula weight	173.33
Crystal system	Monoclinic
Space group	$P2_1/n$
Unit cell dimensions:	
a, Å	11.2513(17)
b, Å	9.9075(16)
c, Å	14.548(2)
β, deg	91.397(3)
Volume, Å^3; Z	1621.2(4); 12
F(000)	1036
θ Range for data collection, deg	2.26–22.10
Limiting indices	$-14 \le h \le 14$,
	$0 \le k \le 12$,
	$0 \le l \le 18$
Reflections collected	13602
Independent reflections (R_{int})	3570 (0.1023)
Numder of refinement	195
Completeness, %	96.5
Goodness-of-fit on F^2	1.077
Final R indices ($I > 2\sigma(I)$)	$R_1 = 0.0846$, $wR_2 = 0.1772$
R indices, all data	$R_1 = 0.1302$, $wR_2 = 0.1990$
$\Delta\rho_{max}/\Delta\rho_{min}$, e Å^{-3}	1.013/−1.060

EXPERIMENTAL

Materials and measurements. All the reagents and solvents for synthesis and analysis were commercially available and used directly. X-ray power diffraction data were recorded on a Rigaku RU200 diffractometer at 60 kV, 300 mA for CuK_α radiation (λ = 1.5406 Å) with a scan speed of 2°C/min and a step size of 0.02° in 2θ. Magnetic susceptibility data of powdered samples restrained in parafilm were measured on Oxford Maglab 2000 magnetic measurement system in the temperature range 300–2 K and at field of 1 kOe.

Synthesis of complex I. A mixture of quaterphenyl-3,3‴,5,5‴-tetracarboxylic acid (H_4L) (0.06 mmol) and $Co(NO_3)_2 \cdot 6H_2O$ (0.1 mmol) and DMF (2 mL) were added into a screw-capped vial. The resulting pink slurry turned clear upon addition of 3 drops of aqueous HNO_3 (63%). The solution was gradually heated to 105°C over a period of 10 h, and kept at this temperature for 3 days. The pink crystalline product was separated by filtration and washed sequentially by DMF, and then dried briefly in air (the yield was 31% base on Co).

IR (KBr; ν, cm^{-1}): 3285 v.s, 2899 w, 2331 m, 1580 v.s, 1398 v.s, 1099 m, 836 m, 786 v.s, 632 m.

X-ray crystallography. Single-crystal X-ray diffraction data for **I** were collected on a Bruker Apex II CCD diffractomete with MoK_α radiation (λ = 0.71073 Å) by using ϕ/ω scan technique at room temperature. The structure was solved by direct methods with SHELXS-97 [43]. The hydrogen atoms were assigned with common isotropic displacement factors and included in the final refinement by use of geometrical restrains. A full-matrix least-squares refinement on F^2 was carried out using SHELXL-97 [43]. The empirical absorption corrections were applied by the SADABS program. The H-atoms of carbon were assigned with common isotropic displacement factors and included in the final refinement by the use of geometrical restraints. The crystallographic data for com-plex **I** are listed in Table 1. Selected bond lengths and angles for **I** are collected in Table 2.

The atomic coordinates and other parameters of the complex have been deposited with the Cambridge Crystallographic Data Center (CCDC no. 1571166; deposit@ccdc.cam.ac.uk).

Photocatalytic method. The photocatalytic reactions were performed as follows. 50 mg of **I** were dispersed in 50 mL aqueous solution of RhB/MV (10 mg/L) under stirring in the dark for 30 min to ensure the establishment of an adsorption-desorption equilibrium. Then the mixed solution was exposed to UV irradiation from an Hg lamp (250 W) and kept under continuous stirring during irradiation for 100 min. Samples of 5 mL were taken out every 10 min and collected by centrifugation for analysis by UV-Vis spectrometer. By contrast, the simple control experiment was also performed under the same condition without adding any catalysts.

RESULTS AND DISCUSSION

The structure was revealed by X-ray analysis and has Co-centered $CoCo_4$ tetrahedra (Fig. 1a). The tetrahedron has one Co ion (Co(3)) at the center, four (Co(1), Co(2), Co(4), and Co(4)^{iv} (^{iv} $3/2 - x$, $-1/2 + y$; $3/2 - z$)) at the apices, and six HCOO groups on the edges. The ligand has one O atom binding the central Co and one apical Co in *syn/anti* mode while other O atom is *syn*-binding one neighboring apical Co atom. By sharing their metal apices these tetrahedra form a 3D framework in which all metal atoms possess octahedral coordination geometry. In the structure Co(3)–Co(4) has two Co–O–Co and one M–O–C–O–M bridges while Co(2)–Co(3) and Co(1)–Co(3) have one Co–O–Co and two M–O–C–O–M bridges. The distances of Co(3)–Co(4), Co(1)–Co(3)

Table 2. Selected bond lengths (Å) and angles (deg) for complex **I***

Bond	*d*, Å	Bond	*d*, Å
Co(1)–O (5)	2.073(8)	Co(1)–O(3)	2.095(8)
Co(1)–O(1)	2.117(7)	Co(2)–O(2)	2.053(8)
Co(2)–O(8)	2.074(9)	Co(2)–O(9)	2.114(7)
Co(3)–O(1)	2.055(8)	Co(3)–O(9)	2.074(6)
Co(3)–O(4)	2.082(7)	Co(3)–O(11)	2.100(7)
Co(3)–O(6)	2.118(8)	Co(3)–O(7)	2.124(7)
Co(4)–O(10)	2.037(7)	Co(4)–O(12)	2.051(8)
Co(4)–O(4)	2.080(7)	Co(4)–O(6)	2.105(7)
Co(4)–O(11)	2.115(7)	Co(4)–O(7)	2.118(7)
Angle	ω, deg	Angle	ω, deg
O(2)Co(2)O(9)	92.1(3)	O(6)Co(3)O(7)	164.2(3)
O(1)Co(3)O(11)	173.0(3)	O(10)Co(4)O(7*A*)	170.9(3)
O(4)Co(4)O(6)	171.8(3)		

* Symmetry transformations used to generate equivalent atoms: (*A*) 3/2 – *x*, 1/2 + *y*, 3/2 – *z*.

and Co(2)–Co(3) are 3.168, 3.513, 3.492 Å, respectively. The open framework has channels running along the *y* direction. The entrance of the channel is about 4.1 × 5.2 Å wide with the exclusion of the van der Waals radii of the surface atoms (Fig. 1b). Complex **I** is an amorphous compound that is formed by dehydrating cobalt formate dehydrates and has been reported in [42]. However, the reported compound from Fu et al., was synthesized by cobalt chloride hexahydrate and excess of 88% formic acid under higher temperature directly. A similar compound is also found by Wang and his co-workers [41].

For **I**, magnetic susceptibility (χ_M) was measured in the temperature range of 2–300 K, and the $\chi_A T$ versus *T* plot is shown in Fig. 2. The observed $\chi_M T$ value at room temperature (3.31 cm^3 K mol^{-1}) was larger than the spin-only value (1.88 cm^3 K mol^{-1}) and close to the value (3.38 cm^3 K mol^{-1}) in case the spin and orbital angular momenta exist independently, suggesting a contribution of the orbital angular momentum. When lowering the temperature, the observed $\chi_M T$ value slightly decreased to show a minimum (2.40 cm^3 K mol^{-1}) at ~5 K, and below 3.5 K the $\chi_M T$ abruptly increased (2.96 cm^3 K mol^{-1}) at 2 K. The decreasing behavior of $\chi_M T$ seems to be typical of $^4T_1$ term magnetism, caused by the first-order orbital angular momentum, and the observed value is thought

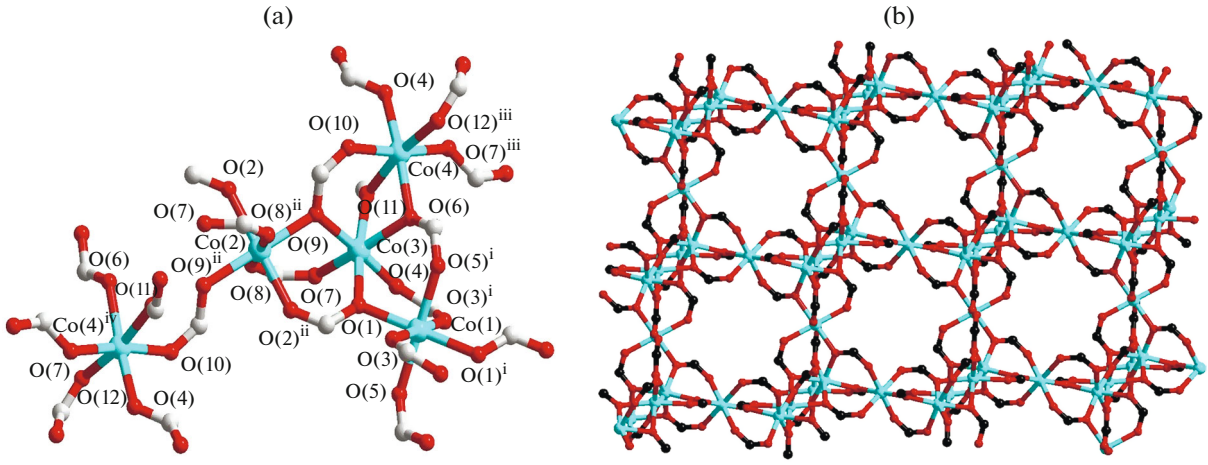

Fig. 1. The coordination geometries of the metal centers and the ligands geometries in **I** (a) (displacement ellipsoids are drawn at the 30% probability level and H atoms are omitted for clarity, symmetric codes: [i] 1 – *x*, 1 – *y*, 1 – *z*; [ii] 2 – *x*, 1 – *y*, 1 – *z*; [iii] 3/2 – *x*, 1/2 + *y*, 3/2 – *z*; [iv] 3/2 – *x*, –1/2 + *y*; 3/2 – *z*); view of the skeleton of **I** along the *y* axis (b).

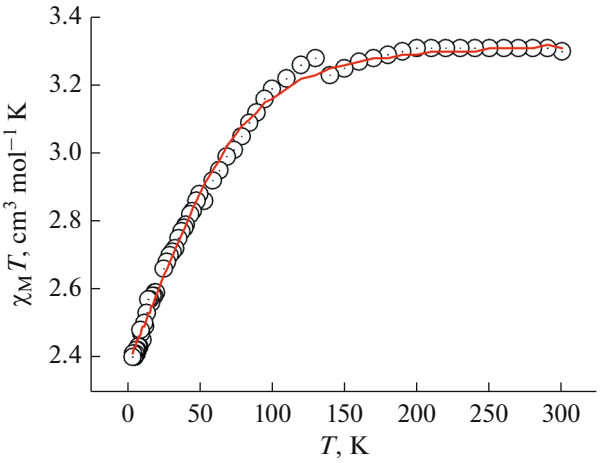

Fig. 2. Plots $\chi_M T$ versus T for **I**, solid lines represent fits to the data.

to be the average of four crystallographically distinguished cobalt(II) ions. Although the structure was too complicated to consider an exact interaction model, the averaged $\chi_M T$ data was successfully fitted by the zero-field splitting model of $S = 3/2$, whose Hamiltonian is written as $H = g_u \beta S_u H_u + D[S_z^2 - S(S+1)/3]$ $(u = x, y, z)$ [44–46]. The magnetic susceptibility equation is as follows:

$$\chi = \frac{\chi_z + 2\chi_x}{3},$$

$$\chi_z = \frac{Ng_z^2\beta^2}{4kT} \frac{1 + 9\exp\left(-\frac{2D}{kT}\right)}{1 + \exp\left(-\frac{2D}{kT}\right)},$$

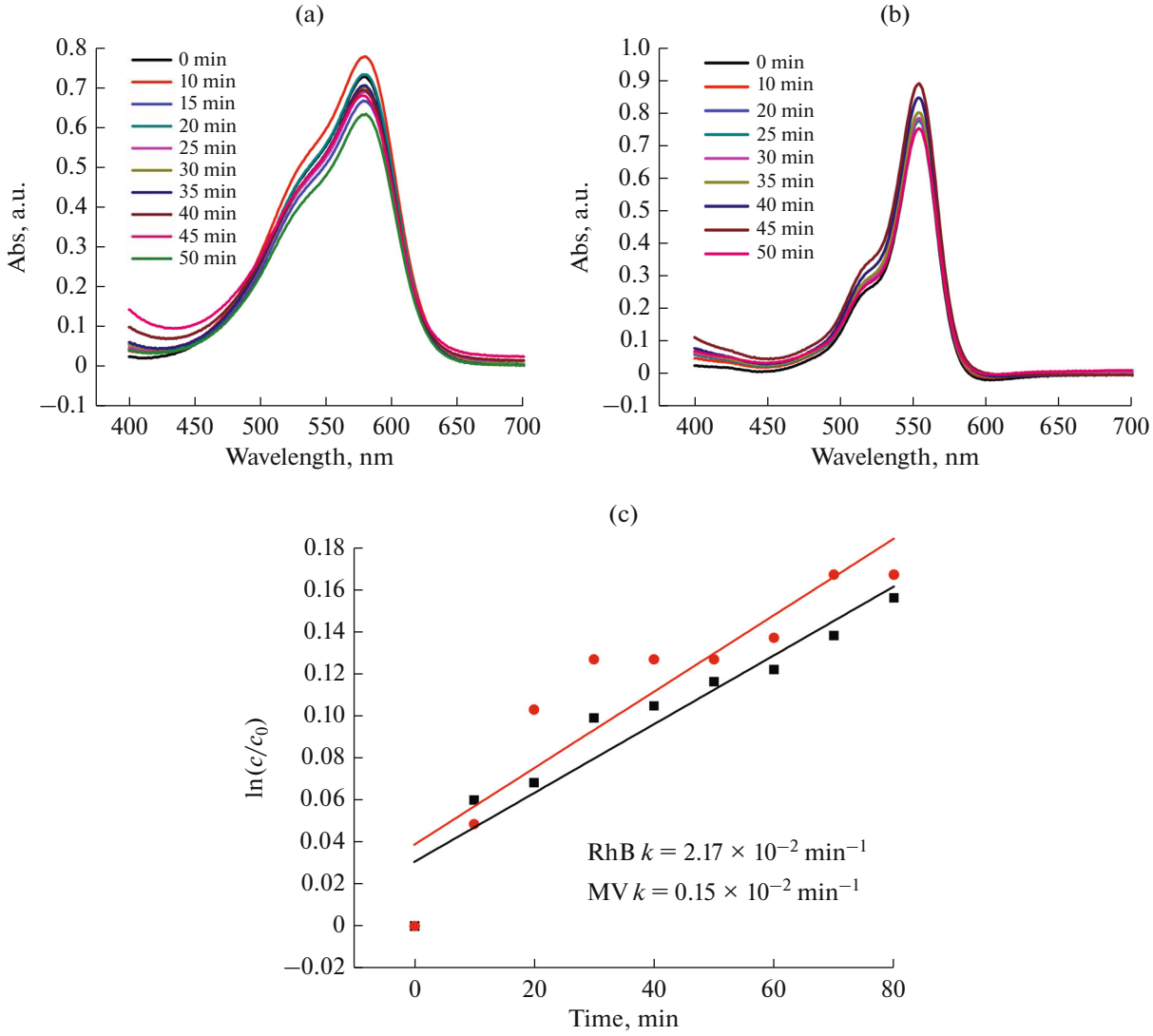

Fig. 3. UV-Vis absorption spectra of the MV (a) and RhB (b) solution during the decomposition reaction under 250 W Hg lamp irradiation in the presence of **I**; photocatalytic degradation kinetics of MV (■) and RhB (●) by **I** (c).

$$\chi_x = \frac{Ng_x^2\beta^2}{kT}\frac{1+\left(\frac{3kT}{4D}\right)\left[1-\exp\left(-\frac{2D}{kT}\right)\right]}{1+\exp\left(-\frac{2D}{kT}\right)}.$$

The best-fitting parameter set was obtained as (D, g_z, g_x, (g_{av})) = (−78.0 cm^{-1}, 2.90, 2.50, (2.64)) with good discrepancy factors ($R_\chi = 9.7 \times 10^{-5}$ and $R_{\chi T} = 6.4 \times 10^{-5}$) in the temperature range of 4–300 K. The abrupt increase in $\chi_M T$ is probably due to the ferromagnetic interaction (or the ferromagnetic phase transition) [47].

The photocatalytic activities of **I** was evaluated by the photo-degradation of MV/RhB in aqueous solution with UV light irradiation using a 250 W Hg lamp. The degradation ratios of MV/RhB dyes in water were monitored by observing the intensity of the characteristic absorption band of MV/RhB. No new absorption band was observed in the UV-Vis absorption spectra, indicating the total decomposition of MV/RhB in water. The absorption peaks of MV and RhB were found to decrease with increasing reaction time for **I** (Fig. 3). The calculation results show that the conversion rates of MV and RhB are 53.45 and 77.08% under UV irradiation, respectively. For the sake of comparison, the total catalytic degradation efficiency of the control experiment (without any catalysts) had also been carried out. The degradation rates of MV and RhB were just 18.2 and 13.3%, respectively, within 50 min under the same condition without catalyst. These results demonstrates that the presence of **I** is necessary for the degradation of MV and RhB. Also, **I** exhibits better photocatalytic activity against MV than that of RhB under similar conditions [48].

To investigate the kinetics of MV/RhB photocatalytic degradation by **I**, experimental data can be described by the Langmuir–Hinshelwood model as expressed by $\ln(c/c_0) = -kt$ (k = apparent reaction rate constant, c_0 is the initial concentration of MV/RhB, t is the reaction time, and c is the concentration of RhB/MV at the reaction time t). The plot of $\ln(c_0/c)$ and irradiation time (t) is approximately linear and approximated the first-order kinetic equation (Fig. 3c). The calculated apparent rate constant k values of RhB and MV are 2.17×10^{-2} and 0.15×10^{-2} min^{-1} for **I**, respectively. Thus, RhB are much higher than that of MV. So, **I** could be chosen as photocatalysts to degrade MV [48, 49].

Thus, we have prepared a Co-formate MOF with Co-centered $CoCo_4$ tetrahedral nodes and open channels. The formate is directed from the decomposition product of dimethyl formamide. The magnetic property shows a main antiferromagnetic interaction and the ferromagnetic phase transition below 2 K. It was found that the photocatalytic decomposition of RhB catalyzed by **I** was faster than those initiated by MV. The better catalytic performance of **I** may be ascribed to adsorption properties for RhB and electronic charges on its solid surface.

ACKNOWLEDGMENTS

This work was partially supported by the Innovation Training Project of Guangdong Medical University (XJ105711445, 2015ZYDM005, and 2015ZZDM007), the College Students Innovation Training Project of Guangdong Province (201710571005, 201710571007, 201710571060, 201710571078, 201710571019), the Science and Technology Plan Key Projects of Dongguan (2012108101010), and Science Foundation funded project of Guangdong Medical University (Z2016001 and M2016023), JSPS KAKENHI grant 15K05445. We also thank Professor Seik Weng Ng for refining the structure and Dr. Y. Wu for measuring the photocatalysis experiments.

REFERENCES

1. Yaghi, O.M., O'Keeffe, M., Ockwig, N.W., et al., *Nature*, 2003, vol. 423, p. 705.
2. Eddaoudi, M., Moler, D.B., Li, H.L., et al., *Acc. Chem. Res.*, 2001, vol. 34, p. 319.
3. Ferey, G., *Chem. Soc. Rev.*, 2008, vol. 37, p. 191.
4. Lin, Z., Slawin, A.M.Z., and Morris, R.E., *J. Am. Chem. Soc.*, 2007, vol. 129, p. 4880.
5. Grzesiak, A.L., Uribe, F.J., Ockwig, N.W., et al., *Angew. Chem. Int. Ed.*, 2006, vol. 45, p. 2553.
6. Zhang, J., Liu, R., Feng, P.Y., et al., *Angew. Chem. Int. Ed.*, 2007, vol. 8388.
7. Burrows, A.D., Cassar, K., Friend, R.M.W., et al., *CrystEngComm*, 2005, vol. 7, p. 548.
8. Yang, S., Lin, X., Blake, A.J.K., et al., *Chem. Commun.*, 2008, p. 6108.
9. Zheng, Y.Q., Lin, J.L., and Kong, Z.P., *Inorg. Chem.*, 2004, vol. 43, p. 2509.
10. Wang, X.F., Zhang, Y.B., Chen, X.N., et al., *CrystEngComm*, 2008, vol. 10, p. 753.
11. Wang, W., Yan, L.Q., Cong, J.Z., et al., *Sci. Rep.*, 2013, vol. 3, p. 1.
12. Xu, G., Zhang, C.W., Ma, X.M., et al., *J. Am. Chem. Soc.*, 2011, vol. 133, p. 14948.
13. Wang, Z.M., Zhang, X.Y., Batten, S.R., et al., *Inorg. Chem.*, 2007, vol. 46, p. 8439.
14. Wang, Z.M., Zhang, B., Inoue, K., et al., *Inorg. Chem.*, 2007, vol. 46, p. 437.
15. Cornia, A., Caneschi, A., Dapporto, P., et al., *Angew. Chem. Int. Ed.*, 1999, vol. 38, p. 1780.
16. Jain, P., Ramachandran, V., Clark, R., et al., *J. Am. Chem. Soc.*, 2009, vol. 131, p. 13625.
17. Jain, P., Dalal, N.S., Toby, B.H., et al., *J. Am. Chem. Soc.*, 2008, vol. 130, p. 10450.
18. And-ujar, M.S., Presedo, S., Yáñez-Vilar, S., et al., *Inorg. Chem.*, 2010, vol. 49, p. 1510.
19. Wang, Z.M., Zhang, B., Otsuka, T., et al., *Dalton Trans.*, 2004, p. 2209.

20. Wang, X.Y., Gan, L., Zhang, S.W., et al., *Inorg. Chem.*, 2004, vol. 43, p. 4615.
21. Stroppa, A., Jain, P., Barone, P., et al., *Angew. Chem. Int. Ed.*, 2011, vol. 50, p. 5847.
22. Hu, K.L., Kurmoo, M., Wang, Z.M., et al., *Chem. Eur. J.*, 2009, vol. 15, p. 12050.
23. Xu, G.C., Ma, X.M., Zhang, L., et al., *J. Am. Chem. Soc.*, 2010, vol. 132, p. 9588.
24. Samantaray, R., Clark, R.J., Choi, E.S., et al., *J. Am. Chem. Soc.*, 2011, vol. 133, p. 3792.
25. Dybtsev, D.N., Chun, H., Yoon, S.H., et al., *J. Am. Chem. Soc.*, 2004, vol. 126, p. 32.
26. Kurmoo, M., Estournès, C., Oka, Y., et al., *Inorg. Chem.*, 2005, vol. 44, p. 217.
27. Hao, X.R., Wang, X.L., Su, Z.M., et al., *Dalton Trans.*, 2009, p. 8562.
28. Qin, M.L., Lee, D.H., and Park, G.J., *Korean. Chem. Soc.*, 2009, vol. 52, p. 73.
29. Han, C.Y., Liu, M.M., and Dang, Q.Q., *Acta Crystallogr., Sect E: Struct. Rep. Online*, 2013, vol. 69, p. 541.
30. Rossin, A., Giambastiani, G., Peruzzini, M., et al., *Inorg. Chem.*, 2012, vol. 51, p. 6962.
31. Lin, X.M., Fang, H.C., Zhou, Z.Y., et al., *CrystEngComm*, 2009, vol. 11, p. 847.
32. Rood, J.A., Noll, B.C., and Henderson, K.W., *Inorg. Chem.*, 2006, vol. 45, p. 5521.
33. Yuan, B.Z., Ma, D.Y., Wang, X., et al., *Chem. Commun.*, 2012, vol. 48, p. 1135.
34. Hao, X.R., Wang, X.L., Su, Z.M., et al., *Dalton Trans.*, 2009, p. 8562.
35. Vaidhyanathan, R., Natarajan, S., and Rao, C.N.R., *Inorg. Chem.*, 2002, vol. 41, p. 4496.
36. Nakagawa, Y., Uehara, K., and Mizuno, N., *Inorg. Chem.*, 2005, vol. 44, p. 9068.
37. Boyle, T.J., Alam, T.M., Tafoya, C.J., et al., *Inorg. Chem.*, 1998, vol. 37, p. 5588.
38. Rood, J.A., Noll, B.C., and Henderson, K.W., *Inorg. Chem.*, 2006, vol. 45, p. 5521.
39. Zhao, H., Qu, Z.R., Ye, Q., et al., *Inorg. Chem.*, 2004, vol. 43, p. 1813.
40. Liu, J.Q., Wu, J., Wang, J., et al., *RSC Adv.*, 2014, vol. 4, p. 20605.
41. Li, M.Y., Kurmoo, M., Wang, Z.M., et al., *Chem. Asian J.*, 2011, vol. 6, p. 3084.
42. Fu, Y.L., Li, M., Shen, X.L., et al., *Acta Crystallogr., Sect. B: Struct. Sci.,* 2005, vol. 61, p. 688.
43. Sheldrick, G.M., *SHELXTL, Version 5.1, Software Reference Manual*, Madison): Bruker AXS, Inc., 1997.
44. Viertelhaus, M., Henke, H., Anson, C.E., et al., *Eur. J. Inorg. Chem.*, 2003, vol. 14, p. 2283.
45. Nakamoto, K., *Infrared and Raman Spectra of Inorganic and Coordination Compounds*, New York: Wiley, 1997.
46. Lines, M.E., *J. Phys. Chem. Solids*, 1970, vol. 31, p. 101.
47. Carter, K.P., Young, A.M., and Palmer, A.E., *Chem. Rev.*, 2014, vol. 114, p. 4564.
48. Wang, X.L., Sun, J.J., Lin, H.Y., et al., *RSC Adv.*, 2016, vol. 6, p. 110583.
49. Wang, L., Shan, Y.X., Gu, X.M., et al., *J. Coord. Chem.*, 2015, vol. 68, p. 2014.